Available online at www.CivileJournal.org

Civil Engineering Journal

Vol. 5, No. 12, December, 2019

# Investigating Role of Vegetation in Protection of Houses during Floods

Amina [a*], Ghufran Ahmad Pasha [a], Usman Ghani [a], Afzal Ahmed [a], Fakhar Muhammad Abbas [a]

[a] *Department of Civil Engineering, University of Engineering and Technology Taxila, Pakistan.*

Received 29 May 2019; Accepted 21 September 2019

**Abstract**

Flood flows have the potential to cause substantial damage to infrastructure, mankind, livestock and agricultural land which all stacks up to greatly affect the financial condition of the region. During 2010 Pakistan floods, more than two million houses were damaged partly or totally [1]. To minimize these types of destructions, inland vegetation can be considered a natural barrier to dissipate the energy of flood flow and limits widespread inundation. This study involves volume of fluid (VOF) modelling approach to figure out the role of vegetation of finite width in energy reduction of flood flow, in front of houses, against: vegetation of varying Aspect Ratio (*A/R* width-length ratio) and distance between vegetation & houses *(Lr)*. Channel domain was built in ANSYS workbench toolkit and meshing was done in meshing building toolkit. For the postprocessing and simulation, FLUENT was used. Various contour plots & profiles of cross stream-wise velocities and water level measurements are presented in this paper. The simulation results of cross stream-wise velocities and water level measurements were identical with experimental data. At vegetation upstream and downstream, velocity reduction observed in higher *A/R* (2.40) compared to vegetation of *A/R*-1. Whereas, outside the vegetation and near the walls of channel domain flow velocities were high. The water level was raised on the upstream side of the vegetation due to resistance offered by vegetation. On the upstream side of vegetation, the rise in backwater depth increased by increasing *A/R*. Contrarily, on the downstream side of vegetation, an undular hydraulic jump was observed in between vegetation and a house. By increasing *A/R*, the energy loss increases under constant vegetation conditions ($G/d$ = 0.24, $Fr_o$ = 0.70; $G$ = spacing of each cylinder in cross-stream direction and $d$= diameter of cylinder and $Fr_o$ = initial Froude number) and increase in house distance from *1W* to *2W*, the energy reduction increased from 2.40% to 3.15% which was further increased to 5.04% for another *5W* increase in house distance, where *W* is the vegetation width. Simulation results also shown that with increasing Froude no from 0.60 to 0.70 water level depth has also an incremental pattern which ultimately results in increase in energy dissipation along the varying building distance (*1W*, *2W* & *5W*). Thus, to minimize the structural damage, a structure must be located at a safe distance away from the vegetation where flow becomes sub-critical.

*Keywords:* VOF Modeling; Vegetation; Flood; k-ε Turbulence Model; Aspect Ratio.

## 1. Introduction

Flood is an enormous amount of water that overflow beyond its normal limits. The impact of floods can cause huge destruction include infrastructure, property and human life. Flood is the increased quantity of fluid (generally water) that inundates the land which is normally dry all year round, from a nearby waterway. Most common inland flood incidents occur near a river or a stream with source of water being a heavy rainfall over a catchment area, either a dam or a levee rupture, or quickly melting snow caps at the mountainous regions. Floods are also caused by tsunamis or hurricanes and that are known as coastal floods as these only do affect the coastal areas and do not travel much distance onto the land. Some notable ones across the world are briefly discussed here. The rise in backwater is increased by both

* Corresponding author: amina168civil@gmail.com

http://dx.doi.org/10.28991/cej-2019-03091436

vegetation density and thickness on upstream side [2]. Vegetations are not only important but multiple factors are important for catastrophic changes during floods [3]. The effect of coastal Vegetation on tsunami run-up heights was investigated and concluded that run up height was reduced by 45% when trees were placed in dense rectilinear arrangement and close to still water level [4]. Critical breaking conditions were used by considering Japanese coastal pine trees. It was observed that inland Vegetations were very helpful to trap much more debris including car debris and large debris [5]. Trees of large diameter can be used to reduce secondary damages caused by driftwood and fluid force intensity [6]. The computational study was given to investigate the flow properties and characteristics. It was observed that velocity was minimum behind the vegetations while in vegetated regions the turbulence was larger, and it was smaller away from the vegetated patch [7].

The analytical model was used to predict the discharge and velocity distribution in compound channel [8]. The flood risk assessment was studied by focusing on frequency analysis (FFA). It was observed that river overflow is more cause of violent variation in flood frequency of downstream areas than dam operations [9]. Non-structural strategies for future flood mitigation in Dhaka city was investigated and concluded that a well-coordinated and balance combination of both structural and nonstructural measures are indispensable for city safety [10]. Vegetation model was used to explain the drag, turbulence and diffusion to unleash the underlying physics, natural range of vegetation density and stem Reynolds' number [11]. The variation of the vegetative roughness coefficient with the depth of flow was studied and it was found that roughness coefficient reduces with increasing depth under the unsubmerged condition and the vegetation roughness tends to increase at low depths under fully submerged condition [12]. Impacts of coastal vegetation on tsunami reduction was studied and observed that when aspect ratio is 1:4, collision effect behind the Vegetation was maximum. While the aspect ratio is fixed, and the vegetation thickness increased, the impact of a collision of the tsunami behind Vegetation becomes more and as result the fluid force increases [13]. Turbulent flow hydraulic properties were studied in an open channel by using three-layer analytical model through suspended vegetation [14]. The drag force is directly proportional to the velocity of flow and mean difference in relationship was due to nature of vegetation [15]. Turbulence was maximum and by increasing depth flow velocity increases [16]. To control the flood flows vegetation can be used. Crops of maize wheat and barley were used as strip cropping pattern [17].

Investigation of damage to mangroves caused by 2004 Indian ocean tsunami in Thailand. It was found that approximately 70% of the mangrove Vegetation was destroyed by tsunami [18]. Experimental work was performed and observed that two rows Vegetation device more driftwood even in sparse case than the single row Vegetation. When aspect ratio is increased it results in devising more driftwood [19].Numerical model was presented by considering the tsunami events of 1975 and 1755 of Portugal and resulted tsunami evacuation maps consisting of safe and quick route, located on high ground to save community [20]. Laboratory experiments were conducted to study the overtopping and its effects on height of inundation behind the structure [22]. Spatio-temporal slip model was used and found that damages of tsunami is due to various inundation features including flow velocity, flow depth [23]. Failure of buildings were due to fluid force and tsunami debris and catastrophic model was proposed to predict accurate damages due to debris. Spatio-temporal model was used to study economical loses to building due to tsunami in Omaha beach New Zealand and concluded that the economic loses to buildings are affected by design and number of buildings [24].Frictional factor in water channel during case of sparse grass was less as compared to dense grass. Dense grass caused more resistance to flow [25]. A study was presented to get more accurate velocity profile using three-dimensional model.it was observed that In case of emergent vegetation velocity was uniform except near the bed due to friction it rapidly increases [26].Flow resistance caused by vegetation was observed and concluded that friction loss in branchy trees is 42 percent greater than the leafless trees and when depth increases it gives more accurate results [27]. Velocity decreases when water flows through vegetation and it was high when it was measured prior to vegetation and this decrease becomes less when we move towards downstream side. Velocity dissipation was dominant in case of flexible vegetation [28]. With increasing depth up to 100 cm forces on the building increases after that they are decreasing because irregularity in flow decreases. When angle on inclination increases, load starts [29]. Performance of different countermeasures for tsunami in Sendai city was investigated and concluded that the combination of greenbelt, seawall and elevated highway and road can protect city [30]. The mean streamwise velocity remain constant inside the larger and shorter vegetation but rises at the top of the vegetation. Also, higher velocities were observed in the vegetation patch regions as compared to the gap regions [31].

In Pakistan, the flood disaster mitigation practices are conventional (i.e. construction of dams, barrages and bunds) and these mostly fail during when a major flood occurs. In rest of the world however, the use of inland vegetation has been introduced as an alternative which is both ecofriendly and does not involve as much capital as required for construction and maintenance of hydraulic structures. The idea arose after looking into Japan's research and their innovations for protection against the tsunami events that occur there in every decade or so. The proposed research is engaged to numerically anticipate the flow behavior in an open channel through emergent vegetation by utilizing k-ε turbulence model. A VOF multiphase method is used in an open channel to predict the velocity distribution and water level measurements in a steady sub critical flow, Also the phenomena of energy loss due to vegetation has been reported as well.

# 2. Martials and Methods

## 2.1. Experimental Conditions

### 2.1.1. Flume Characteristics and Flow Conditions

The experimental data of Pasha and Tanaka (2016) research was used to validate the numerical model [32]. Laboratory experiments were conducted in channel having length 5m, 0.7m in depth and 0.5m in height in Saitama University Japan. Initially the Froude number was initially set 0.7 without vegetation set in a channel and at the channel start the depth of water was set around 4.5cm. The vegetation in staggered arrangement were installed on the channel bed and allocated about 0.75m distance of the channel domain from the from the channel start. Vegetation was displayed as wooden rods with diameter of 0.004m. Using particle image velocimetry (PIV) (Laser Light Sheet: G200, high speed digital CCD camera: K-II, fps: 50–1000, flow analyzing software: FlowExpert2D2C, Katokoken Co., Ltd.) in a cross-wise direction, the velocity distribution at 80% water depth in front of the forest was measured. The flow conditions of the experiment are summarized in Figures 1(a) and 1(b) and Table 1.

**Table 1. Experimental Conditions (32) where (A/R) is aspect ratio, (G/d= spacing of each cylinder in cross-stream direction and d= diameter of cylinder) is vegetation density, ($Fr_o$) is initial Froude number**

| Vegetation A/R | Vegetation Density (cylinders/cm$^2$) | *G/D* | *L/D* | Vegetation Type | $Fr_o$ | Depth (m) | Velocity (m/s) | Cylinder arrangements |
|---|---|---|---|---|---|---|---|---|
| 1.00 | 0.24 | 2.1 | 5.25 | Sparse | 0.70 | 0.45 | 0.465 | Staggered |
| 1.70 | | | | | | | | |
| 2.40 | | | | | | | | |

ANSYS workbench toolkit is used to build the experimental setup. Multizone meshing was done in mesh building toolkit using hexagonal elements. The nodes and elements were different due to different aspect ratio in lateral and vertical directions. The relevance center was used as 20% and 50% according to condition. Mesh independence test was also performed to check independency of grids. Simulation and post-processing were carried out in FLUENT. The channel domain considered of air and water, so volume of fluid model was adopted in postprocessing. The boundary conditions for water inlet and outlet were assigned as velocity inlet and pressure outlet respectively. Side walls, bed, and cylinders of channel domain were considered as no-slip wall to manage the solid walls. The solver type and velocity formulation were chosen as pressure-based and absolute.

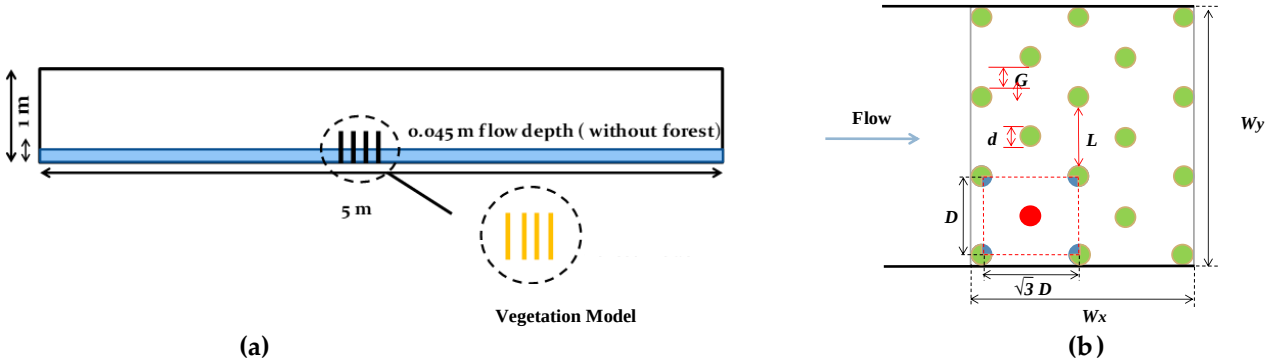


**Figure 1. (a) Experimental model (b) staggered arrangements of vegetation model, where *L* & *G* shows the space between each cylinder in direct-stream and cross-stream direction respectively. *d* is diameter of cylinder, and *Wx* is vegetation length *Wy* is vegetation width**

## 2.2. Governing Equations

Continuity equation, momentum equation and k-ε turbulence equations are the governing equations to represent flow of open channels. For steady incompressible flow these equations are written as:

### 2.2.1. Continuity equation:

The instantaneous continuity equation for an incompressible, homogeneous and steady flow is:

$$\frac{du_i}{dx_i} = 0 \tag{1}$$

### 2.2.2. Momentum Equation

The Naiver-Stokes equation for an incompressible, homogeneous flow is given as:

$$\frac{du_i}{dt} + uj\frac{du_i}{dx_j} = -\frac{1}{e}\frac{\partial \rho}{\partial x_i} + g_i + \upsilon\nabla^2 u_i \quad (2)$$

Where *t* is time, *p* is instantaneous pressure, *gi* is component in the *ith* direction of the gravitational acceleration and *v* is fluid kinematic viscosity.

### 2.2.3. k-ε turbulence model

k-ε turbulence model was used for turbulence modeling. The turbulence kinetic energy k and its dissipation rate ε obtained from the following equations.

For turbulence kinetic energy k:

$$\frac{\partial(\rho k)}{\partial t} + \frac{\partial(\rho k u_i)}{\partial x_i} = \frac{\partial}{\partial x_i}\left[\frac{\mu_t}{\sigma_k}\frac{\partial k}{\partial x_j}\right] + 2\mu_t E_{ij}E_{ij} - \rho\epsilon \quad (3)$$

For turbulent Dissipation rate ε:

$$\frac{\partial(\rho\epsilon)}{\partial t} + \frac{\partial(\rho\epsilon u_i)}{\partial x_i} = \frac{\partial}{\partial x_j}\left[\frac{\mu_t}{\sigma_\epsilon}\frac{\partial \epsilon}{\partial x_j}\right] + C_{1\epsilon}\frac{\epsilon}{k}2\mu_t E_{ij}E_{ij} - C_{2\epsilon}\rho\frac{\epsilon^2}{k} \quad (4)$$

Where

$$\mu_t = \rho C_\mu \frac{k^2}{\epsilon} \quad (5)$$

Where *C*μ is a dimensionless constant. The Equations 3, 4 and 5 comprise of five constants $C_\mu$, $\sigma_k$ , $\sigma_\epsilon$ , $C_{1\epsilon}$ and $C_{2\epsilon}$. The k-ε model utilizes values of these constants as:

$$C_\mu = 0.09, \sigma_k = 1.00, \sigma_\epsilon = 1.30, C_{1\epsilon} = 1.44, C_{2\epsilon} = 1.92. \quad (6)$$

Diffusivities of *k* and ε are linked by Prandtl numbers $\sigma_k$ and $\sigma_\epsilon$ to the eddy viscosity $\mu t$. To measure pressure term of the exact *k*-equation, constants *C*1ε and *C*2ε are used for the correct proportionality between the terms in the *k*- and ε-equations.

## 2.3. Computational Details of Numerical Model

The computational model was built 2m long, 0.7m in width and 0.1m in height. In staggered arrangement the circular cylinders were installed at the middle of the water stream along the width and 0.7m from the upstream side. The diameter of cylinder was taken as 0.004m. The spacing between the circular cylinders was 0.025m and 0.0434m in X direction and Y direction respectively. The meshing around the cylinders was very fine to get good precision and results. Initial average velocity (0.465m/s), water depth (0.045m), height of cylinders (0.1m) are typical hydraulic conditions used for the modeled domain. The *k & ε* turbulence specification method was used into the fluent code, where the turbulence kinetic energy *k* and turbulence dissipation rate *ε* was set to 0.0001220($m^2/s^2$) and 0.00062741($m^2/s^2$). The multi-phase model was used because the channel domain consists of two fluids i.e. water and inlet. The simple scheme & second order upwind discretization scheme were used for pressure-velocity coupling method and VOF multiphase model respectively.

**Table 2. Numerical conditions: where *(A/R)* is aspect ratio, (*G/d*= spacing of each cylinder in cross-stream direction and *d*= diameter of cylinder) is vegetation density, (*Fr)* is initial Froude number, *TKE* is turbulence kinetic energy, *TDR* is turbulence dissipation rate, Lr is house distance, W is width of vegetation**

| Vegetation (*A/R*) | Vegetation Density | *G/D* | *L/D* | Vegetation type | $Fr_o$ | Water depth (y) | velocity (m/s) | Cylindrical arrangement | TKE *(K)* $m/s^2$ | TDR *(ε)* $m^2/s^2$ | *Lr* |
|---|---|---|---|---|---|---|---|---|---|---|---|
| 1 | | | | | 0.7 | | 0.465 | | | | |
| 1.7 | | | | | | | | | | | |
| | 0.24 | 2.1 | 5.25 | sparse | 0.7 | 0.45 m | 0.465 | staggered | 0.000122 | 0.000627 | 1W,2W,5W |
| 2.4 | | | | | 0.65 | | 0.43 | | | | |
| | | | | | 0.6 | | 0.39 | | | | |

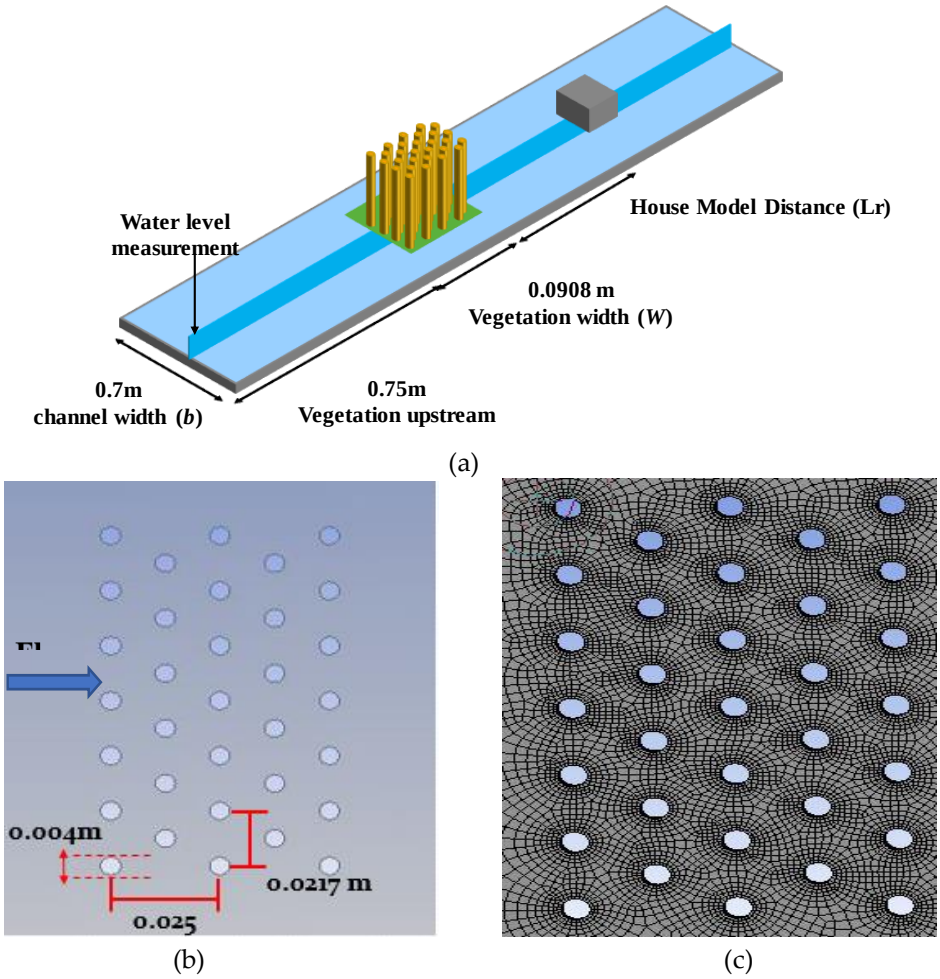


**Figure 2. (a) Schematic diagram of a channel domain (b) arrangement of cylinders in ANSYS Workbench (c) numerical domain mesh (close mesh around cylinders)**

## 3. Results and Discussion

### 3.1. Validation of Numerical Model

#### 3.1.1. Velocity Profiles

At the upstream side of vegetation, the effect of *A/R* on flow velocity is discussed in this section. Different color strips are used to represent the pointed positions of flow velocity as shown in Figure 3. The vegetation is allocated at the center of the channel domain due to which pointed positions were organized on only single side of the Center Line (CL) and conditions are symmetrical to CL. Mean velocity of 1cm strip is represented by Figure 3 for the *A/R* 1, 1.7, 2.4 sparse condition.

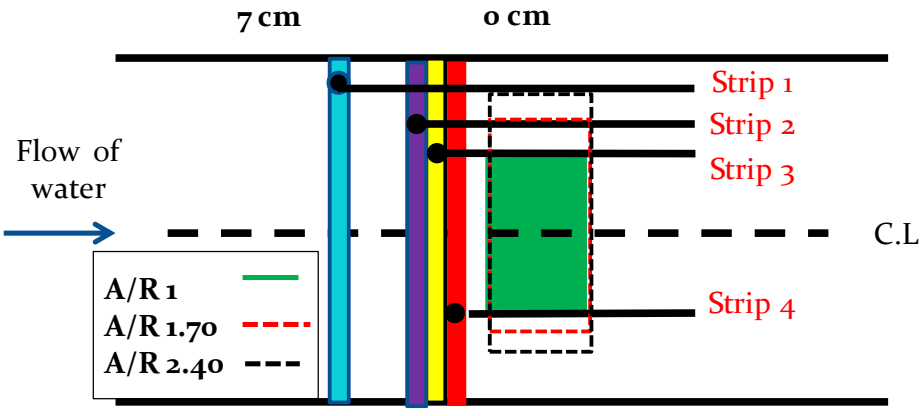


**Figure 3. Location of velocity measurements, the range of velocity measurements (colored strips) from 6-7cm (Strip-1), 3-4 cm (strip-2), 2-3cm (strip-3), and 1-2cm (strip-4), respectively**

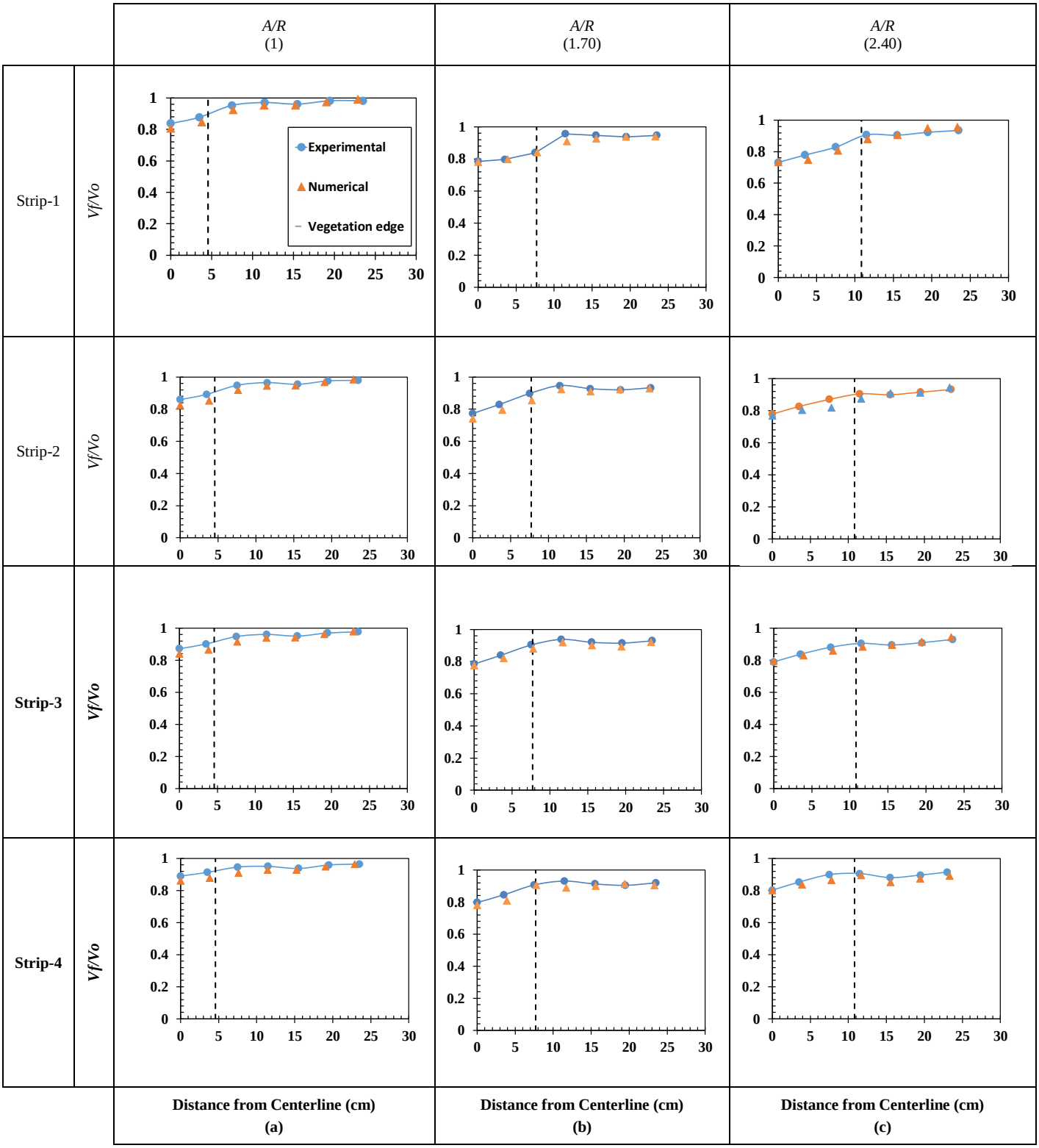


**Figure 4. Comparison of experimental and numerical mean cross-stream wise velocities for sparse case (a) *A/R* 1, (b) *A/R* 1.70, (c) *A/R* 2.40 the x-axis represents mean velocity with and without vegetation and y-axis represents distance from center line of vegetation, the vertical dashed line represents Vegetation edge**

### 3.1.2. Water Level Measurements

The measurement of water level was computed at five dissimilar pointed positions on the upstream side of the vegetation, which are designated by solid black points at the front face of vegetation, and by red points along the length of channel as denoted in Figure 5.

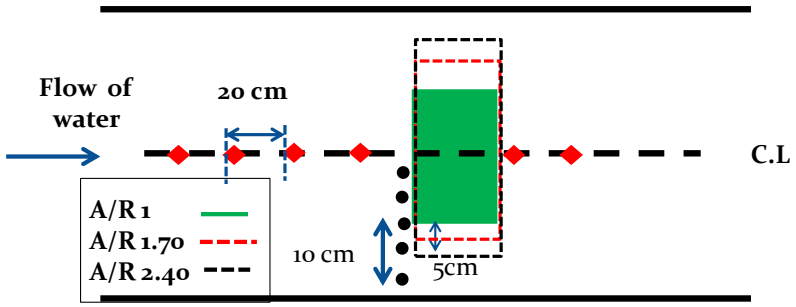


**Figure 5. Location of water level measurements, the zone of water level marked as black circles (front line of vegetation), red circles (center-line of channel domain)**

Increasing the *A/R* of a vegetation the water level was raised to maximum level at the upstream side of vegetation and water surface incline inside the vegetation was also increased. The rise in water level on the upstream side of vegetation mainly depend upon vegetation conditions. The main cause of rise in water level due to resistance offered by vegetation in the path of water outflow. Both the vegetation density and aspect ratio greatly affect the vegetation because a finite length vegetation was used for this case study. The water depth was not consistent throughout the channel therefore the output location was measured at the front of vegetation marked by black circles at five different locations and along the length of channel domain at every 20cm intervals marked by red circles. In Figure 5, assigned as vegetation center, vegetation end, in between the center and end of the vegetation, and 5cm, 10cm away from the vegetation.

Figure 6 represents the water level distribution for sparse case *A/R* (1.0, 1.70, 2.40), vegetation density 0.24 cylinders/cm$^2$. The X-axis shows the distance taken from the channel start and Y-axis shows water level. It is also shown in the Figure 6 that when the vegetation model was mounted in the channel, it results a certain increase of water level at the front of vegetation than outside the vegetation and consequently there is significant rise in water surface slope inside the vegetation. As the *A/R* is increased (keeping the vegetation conditions constant), the water level was raised at the front of vegetation. This rise in the water level depresses the velocity of water flow positively at the front face of the vegetation. Fig 6 also shows that water depth away from the vegetation becomes more as compared to without vegetation.

The water profile in the Figure 6 shows that the simulated results are in better agreement with experimental results. This demonstrated the validity of the numerical model.

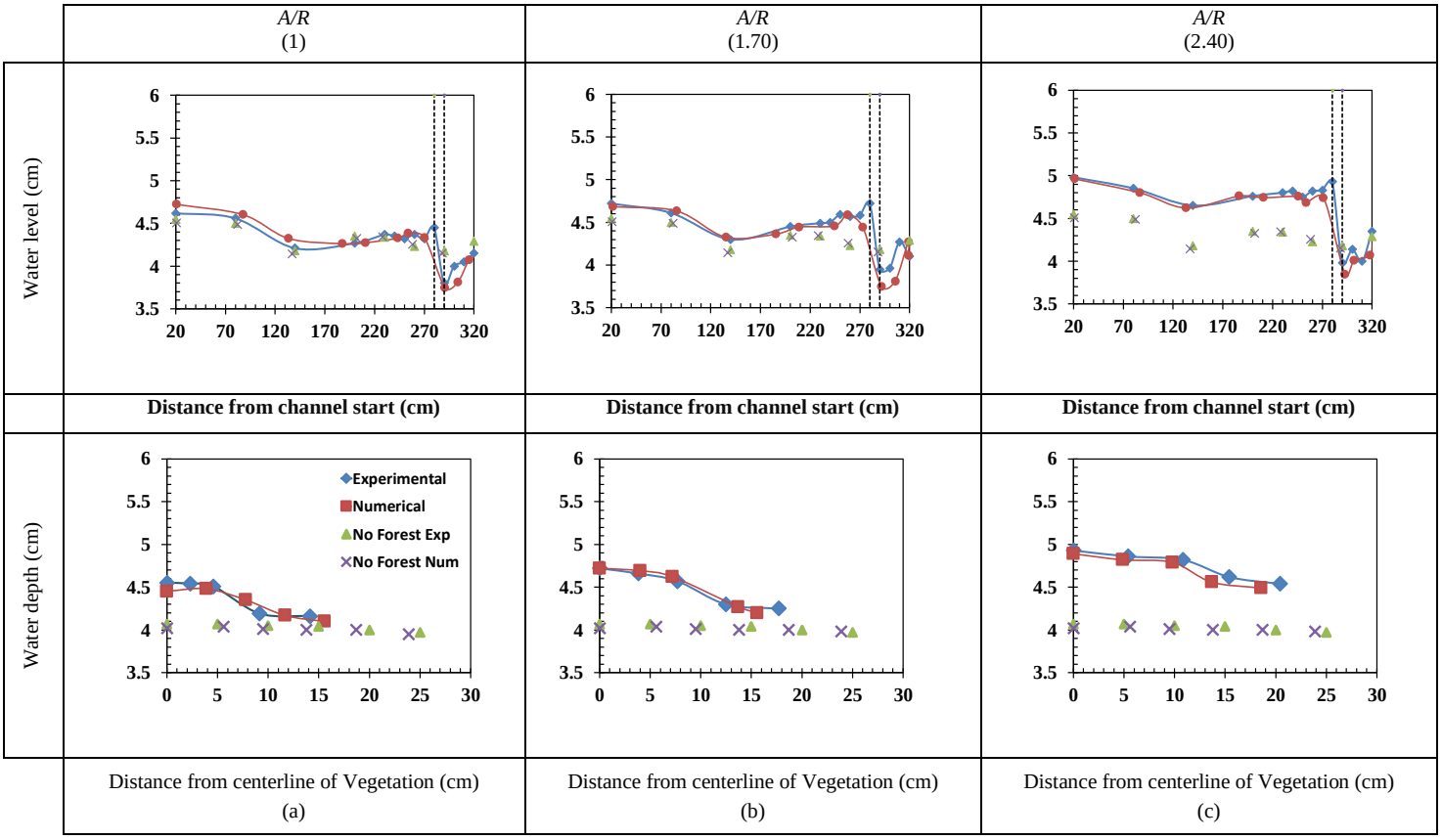


**Figure 6. Water level measurement at the front of vegetation and along the center line of channel (sparse Vegetation), (a) A/R 1.0, (b) A/R 1.70, (c) 2.40, vegetation density: 0.24 Cylinders/cm$^2$ where A/R shows the aspect ratio of vegetation**

## 3.2. Flow Characteristics

### 3.2.1. Velocity Distribution (Upstream and Downstream Location)

The measured positions were figured out only on single side from the central line (CL) for the reason of symmetrical conditions applies to CL as shown in Figure 7. The vegetation model is mounted at the middle of the water channel domain. Therefore, different typical locations were selected to examine the flow properties. The x-axis represents average velocity with vegetation and without vegetation and y-axis represents distance from center line of the vegetation. The vertical dashed line represents vegetation edge in all cases of *A/R* (1, 1.70, 2.40), flow velocity in cross stream-wise direction is initiated to decrease in Strip-1 and it maintained the decreased pattern till approaches to the vegetation. Although the flow was steady, still ripples were observed at the forward-facing of vegetation due to back water rise effect of water. The decrease in the flow velocity is because of the energy reduction inside vegetation area. Increase in *A/R* results a rise in reduction pattern of flow velocity. The larger velocities were observed in Strip-1 because the flow was obstructed to some extent only, whereas the medium velocities were observed in strip (2, 3). The velocity observed higher fluctuations directly upstream of the vegetation at strip 4. (32) have also find the same velocity profiles directly upstream of the vegetation through emergent vegetation. If aspect ratio is increased from *A/R* 1 to *A/R* 2.40 with constant vegetation conditions the flow velocity is decreased because vegetation offered more resistance, there. The velocity magnitude in cross stream-wise direction for all cases of *A/R* (1.0, 1.7, 2.40) directly on the upstream side & downstream side of vegetation are presented in Figure 8.

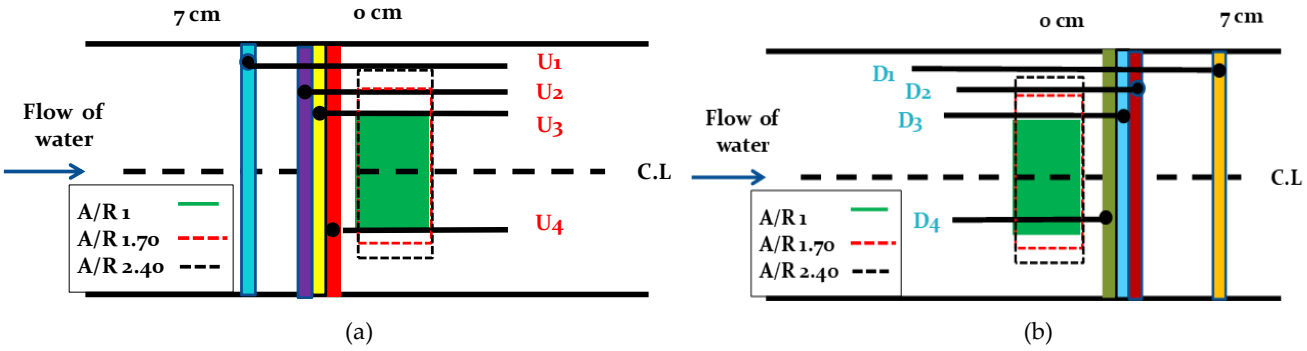


**Figure 7. (a) Area of velocity measurement on the upstream of vegetation (U1, U2, U3, U4) and, (b) downstream vegetation (D1, D2, D3, D4) at five different locations denoted by Different colored strips**

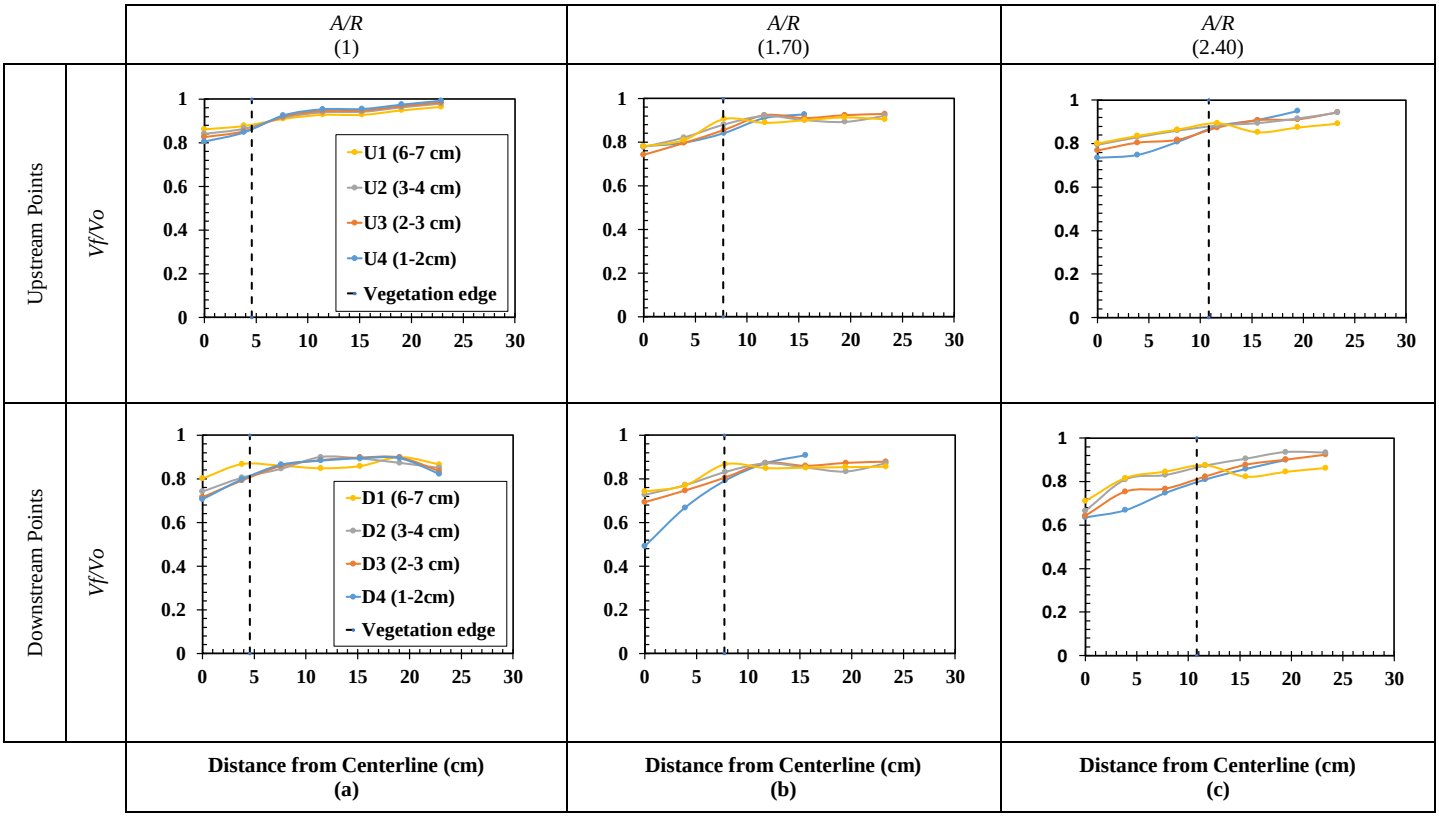


**Figure 8. Mean cross-stream wise velocities, sparse vegetation case, vegetation density 0.24 cylinders/cm$^2$ (a) *A/R* =1 (b) *A/R* 1.70 (c) *A/R* 2.40 upstream location and downstream location**

### 3.3. Water Profiles

These are the water depth profile along the length of the channel measured at the center of channel domain against three different Froude number (0.70, 0.65, 0.60) with constant vegetation conditions. The house models were placed at three different distances (*1W, 2W, 5W*) downstream of the vegetation. These curves follow the scheme of flow shown in Figure 9.

Figure 9 shows clearly shows the backwater rise, undulations in water depth after the vegetation which possibly depicts a undular hydraulic jump and the difference caused to water depth with addition of house at the downstream side of vegetation. The resulting plots show that as distance increases, the difference in depth before and after the vegetation can be seen increasing representing increased energy dissipation. The presence of the building downstream results in increased water depth between the vegetation and building.

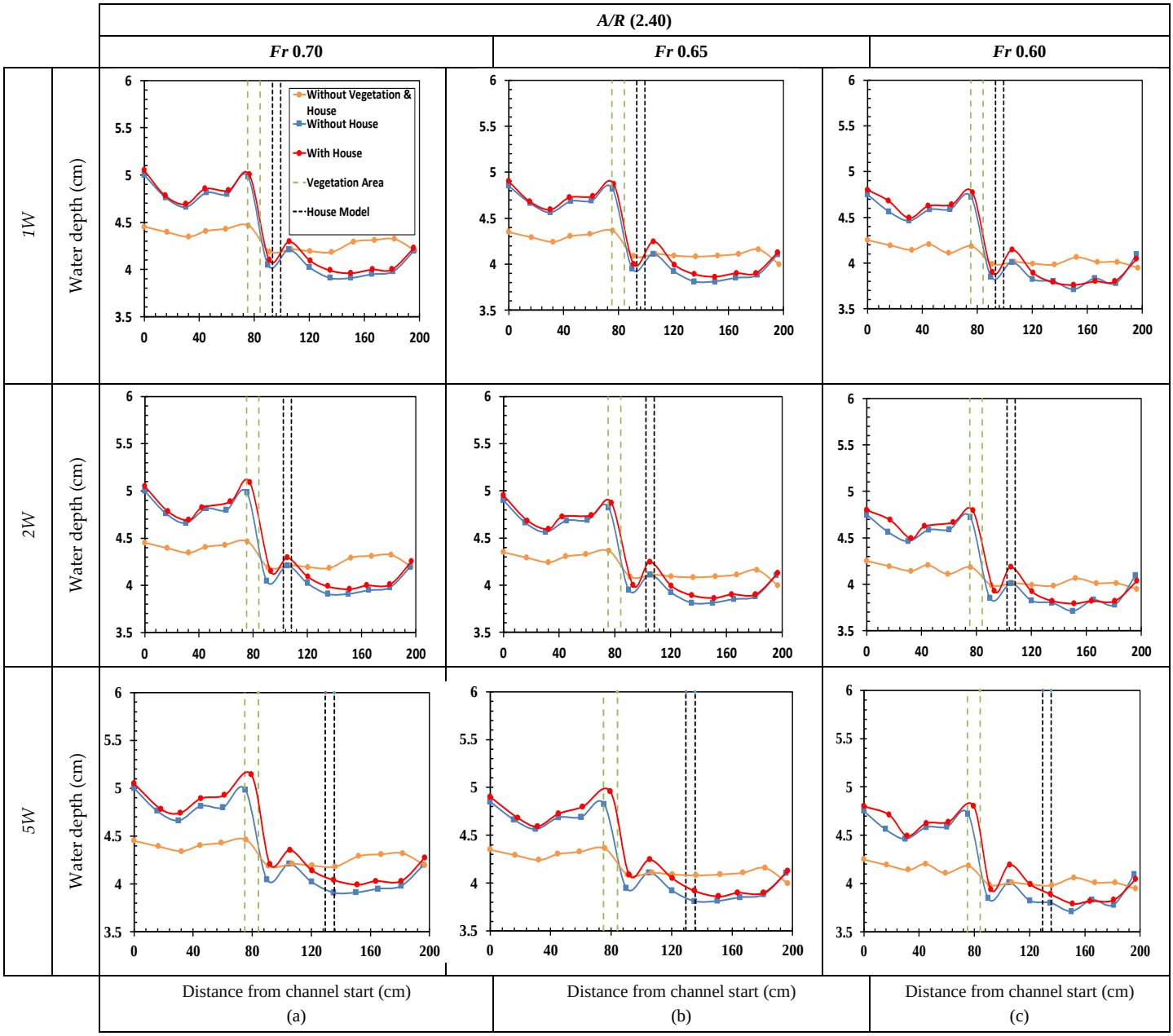


**Figure 9. Water level measurement of channel domain (sparse Vegetation), vegetation density: 0.24 Cylinders/cm$^2$ (a) *A/R* 2.40, *Fr*=0.70, *Lr*= (*1W, 2W, 5W*), (b) *A/R* 2.40, *Fr*=0.65, *Lr*= (*1W, 2W, 5W*), (c) *A/R* 2.40, *Fr*=0.60, *Lr*= *(1W, 2W, 5W)*, where *A/R* shows the aspect ratio of vegetation, green dashed line shows the vegetation area and black dashed line shows the house area**

### 3.4. Contours of Velocity Distribution

The contours of the velocity on the transverse planes for all aspect ratios are captured by the numerical mode as shown in Figures 10 and 11. It can be seen from the Figures 10 and 11 that near the vegetation zone the velocities were reduced. The reduced velocity is because of the vegetation obstruction, because the depth of water was raised directly on the upstream of vegetation. Significant effects of the presence of vegetation was observed on distribution of velocities

within vegetation patch zones, upstream side of vegetation, in the gap region, and near the wall of channel. Maximum amount of velocities was observed in the gap region and near the bed. In all cases of sparse vegetation, vegetation density (0.24 cylinders/cm2), *A/R* (1, 1.7, 2.4), the velocity is started to decrease in strip-1 and follow this reduction pattern till approaches the vegetation.

In *A/R* 1.0 Strip-1 (6-7 cm) the velocity is started to decrease directly upstream of the vegetation and maximum velocity in the gap region and near the walls of channel. In strip 2 (2-3 cm), strip 3 (3-4 cm) the magnitude of velocity is further reduced because this region is near to the vegetation. The legend shows the magnitude of velocity. Similarly, the same behavior is shown in *A/R* 1.7 and 2.40. Hence the contours clearly show that the velocity is reduced in higher *A/R* (2.40) as compared to lesser aspect ratio *A/R (1)*.

By comparing the contours of upstream and downstream sides of the cross stream-wise velocities for sparse case, vegetation density (0.24 cylinders/cm2) and *A/R* (1, 1.70, 2.40), the lower velocities were observed directly at the downstream side of vegetation in comparison to upstream side of vegetation, due to resistance offered by vegetation elements. Average velocities were observed at the middle of channel and maximum velocities were observed away from the vegetation patch.

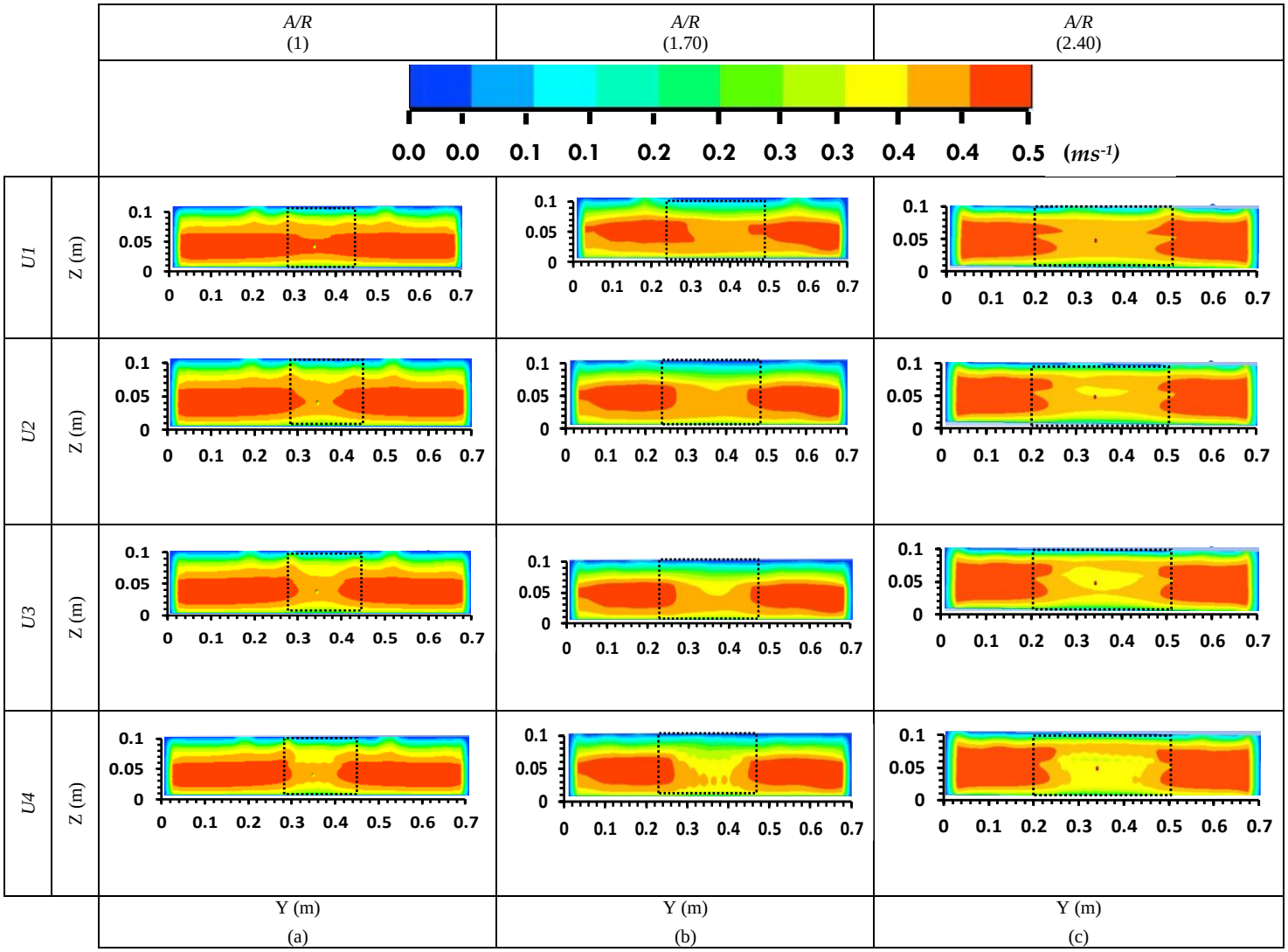


**Figure 10. Contour (upstream location) plots of mean cross stream-wise velocities along the vertical transverse surfaces of all the cases of sparse vegetation, vegetation density 0.24 cylinders/cm$^2$ (a) *A/R*= 1.0, (b) *A/R* =1.70, (c) *A/R* =2.40. The dashed portion show the vegetation patch area**

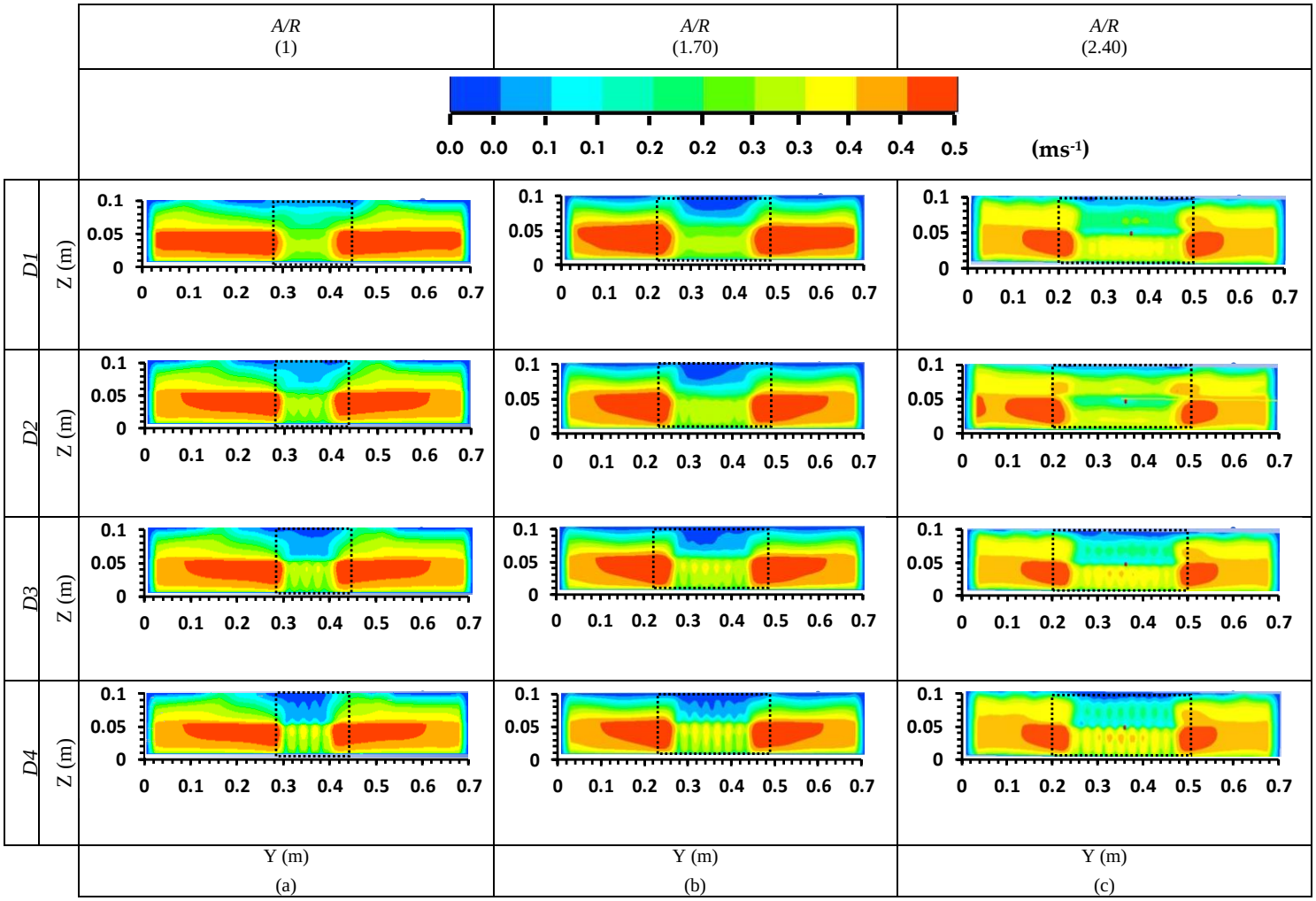


**Figure 11. Contour (Downstream location) plots of mean cross stream-wise velocities along the vertical transverse surfaces of all the cases of sparse vegetation, vegetation density 0.24 cylinders/cm$^2$ (a) *A/R*= 1.0 (b) *A/R* =1.70 (c) *A/R* =2.40. The dashed portion show the vegetation patch area**

### 3.5. Velocity Distribution at the Front of House Model

Figure 12 shows contours obtained at different house distance from vegetation. These plots show that how house distance between vegetation and house model affects in lowering down velocity profiles at downstream side during flood flow. Simulation was carried out at three different house distance: *1W*, *2W*, & *5W*, while keeping *A/R* =2.40. It is clear from the contour plot that velocities are reduced with increasing house distance. So, to get housing safe from flood flow they should be at safe distance from vegetation where flow becomes sub-critical. The reduced velocity profiles along increased house distance results in increased energy dissipation which ultimately make housing safer from flood flow.

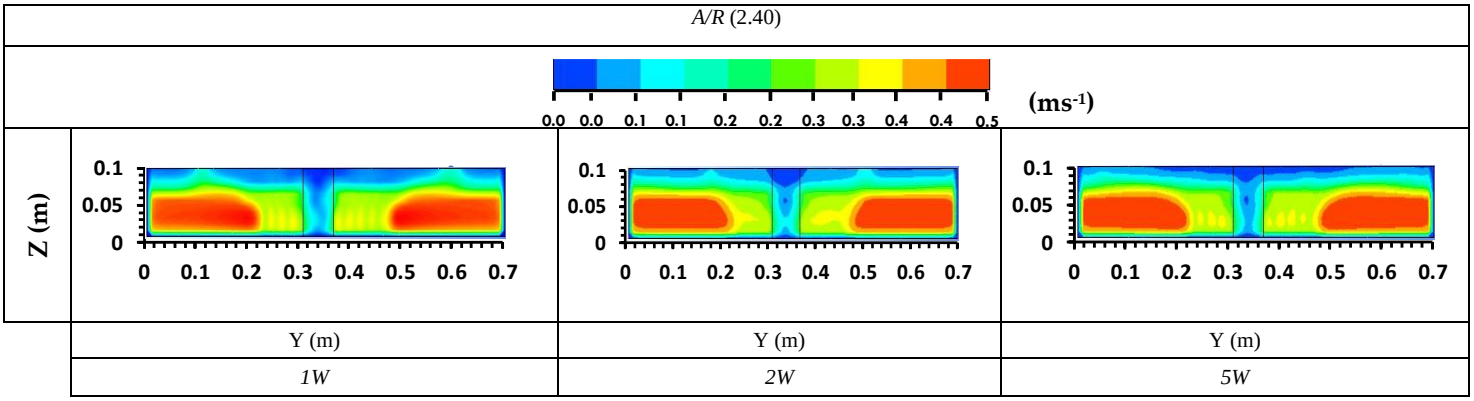


**Figure 12. Contour (Front face of house at section *y*=0.9216 m for *1W*, *y*=1.0124 m for *2W*, *y*=1.2848 m for *5W*) plots of mean cross stream-wise velocities along the vertical transverse surfaces of all the cases of sparse vegetation, vegetation density 0.24 cylinders/cm$^2$, *A/R* =2.40. The dashed portion show the house area**

### 3.6. Energy Dissipation

Relationship between specific energy E, water depth y and velocity V can be shown as [33]:

$$E = y + \alpha \frac{V^2}{g} \quad (7)$$

Where α is velocity variation coefficient and g is gravitational constant. In the current research work α is taken as 1 (2). This equation can be used to find energy dissipation, which is difference between specific energy at the upstream side and downstream side of vegetation. In the present research work, we find Energy dissipation in terms of total energy loss ($\Delta E = E_1 - E_2$) and relative total energy loss ($\Delta E/E$).

#### 3.6.1. Total Relative Energy Loss with Aspect Ratio

Velocity profile and water depth with respect to *A/R* has been shown in Figures 6 and 8. It is clear from Figure 6 that water depth is increasing with increasing *A/R* on the front side of vegetation due to back water rise, also slope of water surface in the vegetation zone increases. As water flow becomes critical on the downstream side through mounted vegetation, a low intensity profile hydraulic jump is created on the downstream side (Figure 13 Flow structure scheme), which ultimately support Energy Loss. Similarly, velocity profile in Figure 8 shows velocity reduction at the downstream side of vegetation than on the upstream side of vegetation, resulting a contribution to Energy Loss.

Extracting data from Figures 6 and 8, a plot of total relative energy loss with respect to *A/R* has been drawn. The *A/R* of vegetation have significant effects on the downstream flow. Increase in the aspect ratio of vegetation causes to reduces the velocity of water at the downstream side of the vegetation and ultimately results in energy loss. Figure 14 shows variation of total energy loss ($\Delta E/E$) with respect to aspect ratio. The relative total energy loss is greatest for sparse case with *A/R* =2.40 and least for *A/R*=1 (i.e. 6.2 and 2.04%) by keeping vegetation density (0.24 cylinders/cm$^2$) and initial Froude number 0.70 constant.

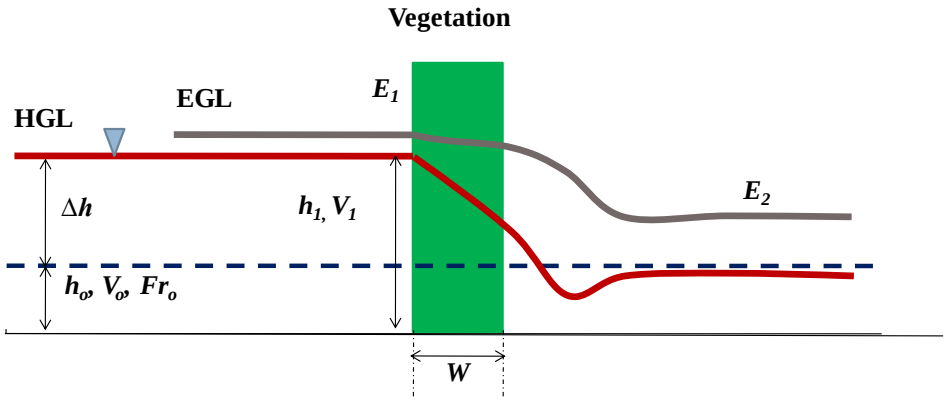


**Figure 13. Flow structure scheme and definition of different parameter**

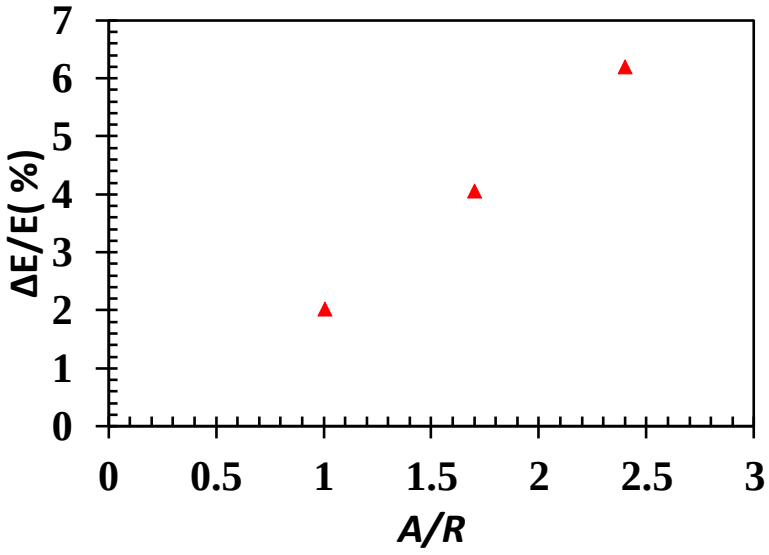


**Figure 14. Relationship between relative total energy loss (ΔE/E) and *A/R* (1, 1.70, 2.40)**

### 3.6.2. Total Relative Energy Loss with Froude Number

Also Figure 16 shows the effect of Froude no. on total relative Energy loss at varying house distance for the single sparse case. It is clear from the Figure 9 that with increasing Froude no, water level depth has also incremental pattern. This increment in water depth ultimately results in increasing energy loss. In Figure 16 curve is drawn for the vegetation model with characteristics: Vegetation Density=0.24 cylinders/cm$^2$ & Froude number =(0.7, 0.65, 0.6). For this single case of vegetation and in between three Froude numbers (0.7, 0.65, 0.6) the energy loss increased exponentially. The increase in building distance from 0.9216m (*1W*) to1.0224m (*2W*) increase the relative total energy loss from 2.40 to 3.15% and when increase to *5W* (1.2948), the energy reduction further increased 5.04%.

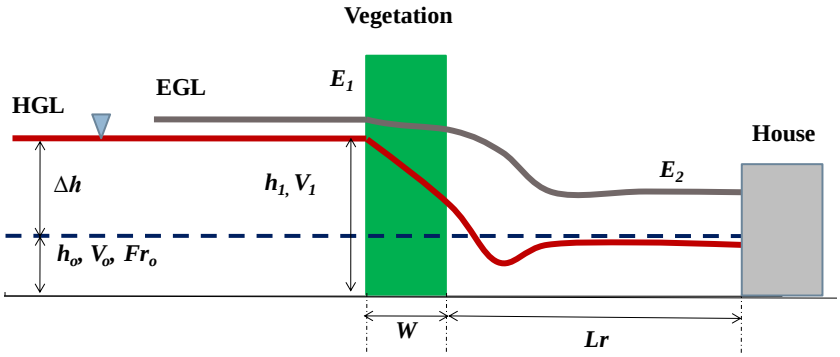


**Figure 15. Flow structure scheme with house model**

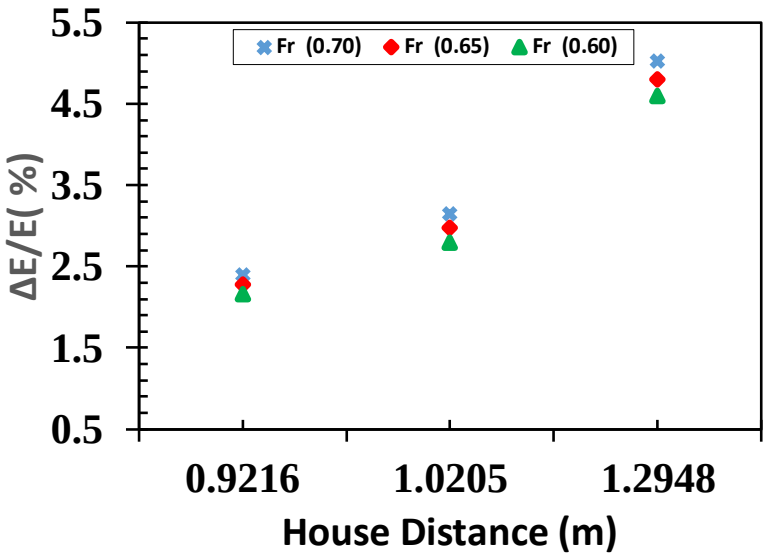


**Figure 16. Relationship between relative total energy loss and house distance**

## 4. Conclusions

In this research work, Velocity distribution, water profiles & Energy dissipation of steady sub critical flow through emergent vegetation have been computed using VOF multi-phase method. A k- $\varepsilon$ turbulence model was used in this study. The research can be concluded as follows:

- A numerical study has been done using Ansys software to predict the mean cross stream-wise velocities in an open channel and water level measurements against three different *A/R* (1, 1.7, 2.40) through emergent vegetation. The simulation results show that multi-zone mesh converges rapidly and have good correspondence between numerical model and experimental results.
- From the contour plots the minimum magnitude of cross stream-wise velocities was found within vegetation zone as compared to the gap regions.
- Velocity profiles and contour plots depicts the reduction in velocities along the upstream side of vegetation as well as in the downstream side of the vegetation. Lower velocities in upstream side were due to back water rise effect while in downstream side it was due to resistance of vegetation elements in the path of flow.
- At the vegetation upstream side, for constant vegetation density (*G/d*), velocity reduction increases with the increase in *A/R* (1.0, 1.70, 2.40) along the channel length. Similarly, the *A/R* of vegetation have significant effects

on the downstream flow. Increase in the aspect ratio of vegetation causes to reduces the velocity of water at the downstream side of the vegetation

- Water depth also increases with increasing A/R from 0.60 to 0.70 along the channel.
- The total relative energy dissipation by the vegetation is greater for the model of higher aspect ratio. Increase in aspect ratio from 1 to 2.40 resulted in more energy reduction from 2.02 to 6.2%.
- The building distance greatly affects the energy dissipation. For constant vegetation conditions and single sparse case (*A/R*=2.4), the increase in building distance from *1W* (0.9297m) to *2W* (1.0205 m), the energy reduction increased from 2.40 to 3.15% which was further increased for distance *5W* (1.2948) i.e. 5.04%
- Simulation results shows the effect of Froude no. on total relative Energy loss at varying house distance for the single sparse case. According to results with increasing Froude no from 0.60 to 0.70 water level depth has also an incremental pattern which ultimately results in increase in energy dissipation along the varying building distance (*1W, 2W & 5W*).

According to the observations, it is recommended that vegetation should be of high aspect ratio for greater energy dissipation and the building should be at a great distance from the vegetation to obtain maximum effect of the vegetation and hence safety

These results are vital for the optimum vegetation design for the protection of structures. In the future, the aim is to do develop a numerical model with different densities of vegetation and other actual ground conditions to find minimum optimum building distance to be observed and followed from the flood plane to reduce flood destructions with vegetation.

## 5. Notations

| | | | |
|---|---|---|---|
| *A/R* | Aspect ratio (width-length) | *Vo* | Average velocity without vegetation |
| *Lr* | House distance | *E* | Specific Energy at forest front |
| *D* | Diameter of cylinder | *y* | Water depth |
| *G* | Spacing of each cylinder in cross stream-wise direction | *V* | Velocity of water (ms-1) |
| $Fr_0$ | Initial Froude number | $\alpha$ | Velocity variation constant |
| *W* | Width of vegetation | *g* | Gravitational constant |
| *L* | Spacing between each cylinder | $\Delta E\%$ | Total energy loss |
| *Wx* | Vegetation length | $\Delta E/E\%$ | Relative total energy loss |
| *Wy* | Vegetation width | $\Delta h$ | water depth with vegetation |
| *TKE* | Turbulence kinetic energy | *ho* | Initial water depth without vegetation |
| *TDR* | Turbulence dissipation rate | *HGL* | Hydraulic Grade Line |
| *m* | meter | *EGL* | Energy Grade line |
| *s* | Second | $E_1$ | Specific Energy at forest front |
| *cm* | Centimeter | $E_2$ | Specific Energy at a point of minimum water depth where the flow is super-critical |
| *Vf* | Average velocity with vegetation | | |

## 6. Acknowledgements

The authors are very thankful to Higher Education Commission (HEC), Pakistan, for the services of Computational Fluid Dynamics (CFD) software at University of Engineering & Technology, Taxila, Pakistan, which was used to perform this research work.

## 7. Conflicts of Interest

The authors declare no conflict of interest.

## 8. References

[1] Shah, Attaullah, Hamid Khan, and Ehsan Qazi. "Damage assessment of flood affected mud houses in Pakistan." Journal of Himalayan Earth Sciences 46, no. 1 (2013).

[2] Pasha, Ghufran Ahmed, and Norio Tanaka. "Undular Hydraulic Jump Formation and Energy Loss in a Flow through Emergent Vegetation of Varying Thickness and Density." Ocean Engineering 141 (September 2017): 308–325. doi:10.1016/j.oceaneng.2017.06.049.

[3] Smith, Bronte. "The role of vegetation in catastrophic floods: A spatial analysis.", University of Wollongong (2013).

[4] Irtem, Emel, Nuray Gedik, M. Sedat Kabdasli, and Nilay E. Yasa. "Coastal Forest Effects on Tsunami Run-up Heights." Ocean Engineering 36, no. 3–4 (March 2009): 313–320. doi:10.1016/j.oceaneng.2008.11.007.

[5] Tanaka, Norio, Junji Yagisawa, and Satoshi Yasuda. "Breaking Pattern and Critical Breaking Condition of Japanese Pine Trees on Coastal Sand Dunes in Huge Tsunami Caused by Great East Japan Earthquake." Natural Hazards 65, no. 1 (September 7, 2012): 423–442. doi:10.1007/s11069-012-0373-4.

[6] Tanaka, Norio, Hajime Sato, Yoshiya Igarashi, Yuya Kimiwada, and Hiroyuki Torita. "Effective Tree Distribution and Stand Structures in a Forest for Tsunami Mitigation Considering the Different Tree-Breaking Patterns of Tree Species." Journal of Environmental Management 223 (October 2018): 925–935. doi:10.1016/j.jenvman.2018.07.006.

[7] Anjum, Naveed, Usman Ghani, Ghufran Ahmed Pasha, Muhammad Usman Rashid, Abid Latif, and M. Zubair Yousaf Rana. "Reynolds Stress Modeling of Flow Characteristics in a Vegetated Rectangular Open Channel." Arabian Journal for Science and Engineering 43, no. 10 (April 2, 2018): 5551–5558. doi:10.1007/s13369-018-3229-8.

[8] Jiang, Beihan, Kejun Yang, and Shuyou Cao. "An Analytical Model for the Distributions of Velocity and Discharge in Compound Channels with Submerged Vegetation." Edited by Vanesa Magar. PLOS ONE 10, no. 7 (July 10, 2015): e0130841. doi:10.1371/journal.pone.0130841.

[9] Tanaka, Tomohiro, Yasuto Tachikawa, Yutaka Ichikawa, and Kazuaki Yorozu. "Impact Assessment of Upstream Flooding on Extreme Flood Frequency Analysis by Incorporating a Flood-Inundation Model for Flood Risk Assessment." Journal of Hydrology 554 (November 2017): 370–382. doi:10.1016/j.jhydrol.2017.09.012.

[10] Faisal, I.M, M.R Kabir, and A Nishat. "Non-Structural Flood Mitigation Measures for Dhaka City." Urban Water 1, no. 2 (June 1999): 145–153. doi:10.1016/s1462-0758(00)00004-2.

[11] Nepf, H. M. "Drag, Turbulence, and Diffusion in Flow through Emergent Vegetation." Water Resources Research 35, no. 2 (February 1999): 479–489. doi:10.1029/1998wr900069.

[12] Wu, Fu-Chun, Hsieh Wen Shen, and Yi-Ju Chou. "Variation of roughness coefficients for unsubmerged and submerged vegetation." Journal of hydraulic Engineering 125, no. 9 (1999): 934-942. doi:10.1061/(ASCE)0733-9429(1999)125:9(934).

[13] Iimura, Kosuke, and Norio Tanaka. "Numerical Simulation Estimating Effects of Tree Density Distribution in Coastal Forest on Tsunami Mitigation." Ocean Engineering 54 (November 2012): 223–232. doi:10.1016/j.oceaneng.2012.07.025.

[14] Huai, Wenxin, Yang Hu, Yuhong Zeng, and Jie Han. "Velocity Distribution for Open Channel Flows with Suspended Vegetation." Advances in Water Resources 49 (December 2012): 56–61. doi:10.1016/j.advwatres.2012.07.001.

[15] Schoneboom, Thomas, Jochen Aberle, and Andreas Dittrich. "Hydraulic resistance of vegetated flows: Contribution of bed shear stress and vegetative drag to total hydraulic resistance." River Flow 2010 (2014): 269-276.

[16] Carollo, Francesco Giuseppe, V. I. T. O. Ferro, and D. Termini. "Flow velocity measurements in vegetated channels." Journal of Hydraulic Engineering 128, no. 7 (2002): 664-673. doi:10.1061/(ASCE)0733-9429(2002)128:7(664).

[17] Smith, R.J., N.H. Hancock, and J.L. Ruffini. "Flood Flow through Tall Vegetation." Agricultural Water Management 18, no. 4 (November 1990): 317–332. doi:10.1016/0378-3774(90)90014-p.

[18] Tanaka, Norio, and Junji Yagisawa. "Effects of Tree Characteristics and Substrate Condition on Critical Breaking Moment of Trees Due to Heavy Flooding." Landscape and Ecological Engineering 5, no. 1 (January 15, 2009): 59–70. doi:10.1007/s11355-008-0060-5.

[19] Pasha, Ghufran Ahmed, Norio Tanaka, Junji Yagisawa, and Fuadi Noor Achmad. "Tsunami Mitigation by Combination of Coastal Vegetation and a Backward-Facing Step." Coastal Engineering Journal 60, no. 1 (January 2, 2018): 104–125. doi:10.1080/21664250.2018.1437014.

[20] Santos, Angela, Nuno Fonseca, Margarida Queirós, José Zêzere, and José Bucho. "Implementation of Tsunami Evacuation Maps at Setubal Municipality, Portugal." Geosciences 7, no. 4 (November 8, 2017): 116. doi:10.3390/geosciences7040116.

[21] Wüthrich, Davide, Michael Pfister, Ioan Nistor, and Anton J. Schleiss. "Effect of Building Overtopping on Induced Loads During Extreme Hydrodynamic Events." Journal of Hydraulic Research (March 29, 2019): 1–16. doi:10.1080/00221686.2019.1573764.

[22] Adriano, Bruno, Satomi Hayashi, and Shunichi Koshimura. "Analysis of Spatio-Temporal Tsunami Source Models for Reproducing Tsunami Inundation Features." Geosciences 8, no. 1 (December 25, 2017): 3. doi:10.3390/geosciences8010003.

[23] Macabuag, Joshua, Tiziana Rossetto, Ioanna Ioannou, and Ian Eames. "Investigation of the Effect of Debris-Induced Damage for Constructing Tsunami Fragility Curves for Buildings." Geosciences 8, no. 4 (March 31, 2018): 117. doi:10.3390/geosciences8040117.

[24] Paulik, Ryan, Emily Lane, Shaun Williams, and William Power. "Changes in Tsunami Risk to Residential Buildings at Omaha Beach, New Zealand." Geosciences 9, no. 3 (March 2, 2019): 113. doi:10.3390/geosciences9030113.

[25] Chiew, Yee-Meng, and Soon-Keat Tan. "Frictional resistance of overland flow on tropical turfed slope." Journal of hydraulic engineering 118, no. 1 (1992): 92-97. doi:10.1061/(ASCE)0733-9429(1992)118:1(92).

[26] Gao, Guanghai, Roger A. Falconer, and Binliang Lin. "Modelling open channel flows with vegetation using a three-dimensional model." Journal of Water Resource and Protection 3, no. 02 (2011): 114.

[27] Järvelä, Juha. "Determination of Flow Resistance Caused by Non‐submerged Woody Vegetation." International Journal of River Basin Management 2, no. 1 (March 2004): 61‐70. doi:10.1080/15715124.2004.9635222.

[28] Meftah, M. Ben, F. De Serio, D. Malcangio, A. F. Petrillo, and M. Mossa. "Experimental study of flexible and rigid vegetation in an open channel." In Proc. River Flow, vol. 1 (2006): 603-611.

[29] Cuomo, Giovanni, Gholamreza Shams, Sebastian Jonkman, and Pieter van Gelder. "Hydrodynamic Loadings of Buildings In Floods." Coastal Engineering 2008 (May 2009): 3744–56. doi:10.1142/9789814277426_0310.

[30] Pakoksung, Kwanchai, Anawat Suppasri, and Fumihiko Imamura. "Systematic Evaluation of Different Infrastructure Systems for Tsunami Defense in Sendai City." Geosciences 8, no. 5 (May 10, 2018): 173. doi:10.3390/geosciences8050173.

[31] Anjum, Naveed, Usman Ghani, Ghufran Ahmed Pasha, Abid Latif, Tahir Sultan, and Shahid Ali. "To Investigate the Flow Structure of Discontinuous Vegetation Patches of Two Vertically Different Layers in an Open Channel." Water 10, no. 1 (January 16, 2018): 75. doi:10.3390/w10010075.

[32] Pasha, Ghufran Ahmed, and Norio Tanaka. "Effectiveness of Finite Length Inland Forest in Trapping Tsunami-Borne Wood Debris." Journal of Earthquake and Tsunami 10, no. 04 (October 2016): 1650008. doi:10.1142/s1793431116500081.

[33] Chow, Ven T. "Open-channel hydraulics." McGraw-Hill Civil Engineering Series, McGraw-Hill: Tokyo. xviii, 680 pp. (1959).